MoS2 "inorganic fullerenes" combined with TiO2 in water-methanol suspensions: Highly active hydrogen production photo catalysts operating via transfer of accumulated electrons

P. Afanasiev

MoS_2 "inorganic fullerenes" combined with TiO_2 in water-methanol suspensions: highly active hydrogen production photo catalysts operating via transfer of accumulated electrons.

Pavel Afanasiev

Institut de Recherches sur la Catalyse et l'Environnement de Lyon IRCELYON, UMR 5256, CNRS – Université Lyon 1, 2 av A. Einstein 69626 Villeurbanne Cedex (France); Fax: 33 04 7244 5399; Tel: 33 04 72 44 5466;

E-mail: pavel.afanasiev@ircelyon.univ-lyon1.fr

ABSTRACT

Water-methanol suspensions of size-tuned hollow MoS_2 "inorganic fullerenes" (IF) combined with high surface area anatase TiO_2 efficiently promote photo catalytic hydrogen evolution reaction (PHER). Despite low amount of the MoS_2 slabs edges in the structure of closed-shell IF-MoS_2 particles and relatively poor dispersion of co-catalyst, the best composite catalysts were nearly 50% as active as Pt/TiO_2 benchmark and considerably more active than the reference MoS_2-TiO_2 catalysts containing highly dispersed MoS_2 slabs. Straightforward experimental evidence is given that hydrogen is formed due to transfer of trapped (accumulated) electrons from the TiO_2 particles to the IF-MoS_2 particles in liquid suspension. Electrochemical flat band potential measurements support the possibility of electrons transfer from TiO_2 to IF-MoS_2.

Keywords: Titanium oxide; Molybdenum sulfide; Photocatalysis; Hydrogen production; Inorganic fullerenes

1. Introduction

Photocatalytic hydrogen evolution reaction (PHER) over semiconductor photocatalysts for converting solar energy into H_2 chemical energy is among the most intensely developing research topics [1, 2]. Despite a tremendous effort to develop alternative materials, titanium oxide (TiO_2) remains arguably the most efficient semiconductor for PHER, because it combines low cost, high stability and excellent activity under UV irradiation [3, 4]. Many studies are directed on the PHER using organic molecules as hole scavengers, one on the most popular among them being methanol [5]. As the reaction rate on bare titania is low, a co-catalyst is

usually added to titania in order to accelerate hydrogen release. PHER using methanol or methanol-water mixtures and TiO_2 semiconductor has been tried with a wide range of co-catalysts, the noble metals (Pt, Pd, Au) being the most active [6].

As an alternative to noble metals, sulfides of transition metals are widely studied, in particular lamellar MoS_2 and WS_2 [7]. Different techniques have been applied to prepare MoS_2-TiO_2 photo catalysts, such as mechanochemical [8], solvothermal [9] and others. The works on the MoS_2-TiO_2 composites have been recently reviewed [10]. With many respects, the design of PHER catalysts is inspired by the research carried out in the field of (photo)electro catalytic HER cells (PEC) on one side and in the heterogeneous catalysis on the other side. The role of fine dispersion of MoS_2 and the necessity of its good interaction with the substrate is emphasized for the MoS_2 materials developed for PEC or for lithium batteries [11, 12]. In the same lines, the importance of a tight contact between the TiO_2 surface and highly dispersed MoS_2 co-catalyst for PHER has been postulated [13]. In order to improve the quality of contact between two phases and to facilitate the charge transfer, versatile methods have been applied. For example, MoS_2 supported on TiO_2 with face-selected epitaxial deposition was prepared [14] or MoS_2/TiO_2 composites were additionally doped with 1D and 2D conductors, such as exfoliated graphite or CNTs [15]. As the electric resistance along the basal plane of MoS_2 is three orders of magnitude smaller than perpendicularly to the stacked layers [16,17], the MoS_2 fringes connected by edges to the TiO_2 semiconductor have been fabricated in order to improve the electrons transfer [18].

However, despite a great number of studies, the optimal design parameters of TiO_2 semiconductor and MoS_2 co-catalyst as well as their optimal interaction that would provide the highest PHER rates are still not totally clear. The problem is overly complex, due to the multitude of PHER process steps and to a large gap between lifetime scales of charge carriers, trapped species and the characteristic time of chemical reactions. By this reasons the common knowledge acquired in heterogeneous catalysis and PEC research seems to be not directly transposable on PHER. Thus, we previously observed that lesser dispersion of MoS_2 provides higher PHER activity at equal MoS_2 loadings [19]. Additional insights are therefore necessary into the interactions of MoS_2 and TiO_2 and their influence on the PHER efficiency.

For the fundamental understanding of the properties–activity relationships, onion-like or hollow MoS_2 particles, also known as inorganic fullerenes (IF-MoS_2) [20] seem very interesting, as they possess particular properties and provide unique possibility of morphology control. Several techniques were proposed for IF-MoS_2 synthesis, including oxides sulfidation, [21, 22] laser ablation [23] or metal-organic CVD [24]. Recently size controlled fullerenes have been

prepared in a wide range of temperatures, which allows fine tuning of the slabs curvature and of the defects concentration [25].

From the viewpoint of current paradigm dominating PHER research, the IF-MoS_2 materials are expected to be poor PHER co-catalysts for TiO_2. Indeed, IF-MoS_2 particles of ≥ 20 nm size should be considered as poorly dispersed, if compared with short and weakly stacked 3-5 nm MoS_2 slabs supported on TiO_2, available from standard impregnation technique. Moreover closed-shell IF-MoS_2 particles preferentially expose chemically inert basal planes. The IF-MoS_2 surfaces expose quite low (residual) amounts of slabs edges and therefore have lower electrochemical HER efficiency than optimized highly dispersed MoS_2, even if non-negligible catalytic activity of curved and/or broken basal planes IF-MoS_2 was demonstrated [26].

In the present study we report on the unexpectedly high HER activity of mixed IF-MoS_2 - TiO_2 water-methanol slurries, which are at the level of the best photocatalysts of this type ever reported. Then we demonstrate that an essential step of the PHER mechanism in these systems includes transfer of long-live accumulated electrons between TiO_2 and IF-MoS_2 particles.

2. Experimental

2.1.1. Preparation of IF-MoS_2 materials.

The IF-MoS_2 materials were prepared as described in ref. [25]. In brief, size-tuned Scheelites $AMoO_4$ (A=Ca, Sr, Ba) nanoparticles (NP) were prepared and then transformed into hollow sulfide particles. Scheelites NP of varable size were obtained from non-aqueous metathesis as described previously [27]. To prepare the IF-MoS_2 materials, Scheelites NP were treated in a quartz reactor under gas flow containing H_2S and CCl_4, in the temperature range 450 -750 °C.

To prepare the IF-MoS_2 water –methanol suspensions, after cooling and inerting, the freshly sulfided solid (ca. 1 g) was washed upon stirring with 200 ml of distilled water purged with bubbling nitrogen. The washing was repeated several times to remove soluble chloride MCl_2 (M=Ca, Sr, Ba), until negative $AgNO_3$ test. Then distilled water was replaced with methanol or water –methanol mixture and the sample was treated with ultrasound for 1h in an ultrasonic cleaner bath BPAC 120 W. As a result of sonication stable dark suspension was obtained. To remove agglomerates and to provide better size uniformity, the suspension was centrifuged for 10 min at 3000 s^{-1}. The precipitate was discarded whereas the remaining suspension was further utilized as a source of IF-MoS_2 particles. The overall yield of IF-MoS_2 remaining in the suspension depended on the gas-phase reaction temperature and on the type of precursor, but

stayed between 30 and 60 %. The IF-MoS_2 materials are designated as IF-MoS_2–xx-xxx, where xx is the (precursor) particle size and xxx is the preparation temperature (°C), Table S1.

To prepare mixed suspensions, weighted amount of CristalACTiV^{TM} PC500 anatase TiO_2 or other titania powder was dispersed by ultrasound, to give a concentrated 50 g/L aqueous slurry. Then an aliquot of IF-MoS_2 suspension was added and sonication was continued for additional 10 min. The suspension was kept for several hours, which resulted in decantation of the solid, leaving a clear liquid phase. The ultrasound treatment and decantation was repeated in pure methanol and then methanol was added up to obtain 20 g/L slurry of the catalyst. For the catalytic experiments, this concentrated mixture was rapidly re-dispersed by ultrasound and mixed with calculated amounts of water and methanol.

"Deposited" 1% MoS_x/TiO_2 solid was prepared by means of aqueous deposition of MoS_x using thioacetamide as a sulfur source [19]. The preparation technique for "deposited" solids is a simplified version of hydrothermal method by Liu et al [28]. The reference bulk MoS_2 was prepared from the decomposition of ammonium thiomolybdate (ATM) at 450 °C as described in [25]. The benchmark reference catalyst 0.5 wt.% Pt/TiO_2 was prepared by impregnation, drying and reduction with H_2, as described in [29].

2.2. Characterizations

Transmission electron microscopy (TEM) was carried out on a JEOL 2010 device with an accelerating voltage 200 keV. The samples were dispersed in ethanol by ultrasound and then put onto a lacey carbon on a copper grid. The analysis of images was carried out using Gatan Digital Microgtaph™ software. Nitrogen adsorption isotherms were measured on a Micromeritics ASAP 2010 instrument. Specific surface area was determined using BET equation. Prior to measurements, the samples were outgassed in vacuum at 300 °C for 4h. The Mo content in the solids was determined, after dissolution in a HNO_3/H_2SO_4 mixture, by plasma-coupled atomic emission spectroscopy (ICP-ES Activa Jobin Yvon). Elemental analysis of light elements (CHNS) was performed on an analyzer Thermo Fisher Flash 2000.

Hydrodynamic size distribution was measured using Dynamic Light Scattering (DLS) on a Wyatt Nanostar device. Aqueous suspensions containing 0.25 – 0.5 g/L of solids were applied for the DLS measurements. Size distribution was obtained from averaging 10 series of 100 single measurements, 2 s each. Autocorrelation function was cut below 1.5 and above 1500 nm. Surface areas were measured by low temperature nitrogen adsorption and calculated using BET equation.

Zeta- potential (ZP) was determined from electrophoretic mobility in aqueous suspensions on a CAD Zetacompact device. Weighted amounts of powders about 100 mg of were ultrasonically dispersed in 200 ml of 10^{-3} M KNO_3 solution. The pH values were adjusted with either $HClO_4$ or KOH 0.1 M solutions. Electrophoretic migration rate was converted to zeta potential by the Helmholtz-Smoluchowski equation. Low values of ZP close to IEP are highly uncertain since the mobility is influenced by current-induced flows, making the apparent ZP strongly dependent on the laser position. To decrease uncertainty, at each pH we determined ZP in several points outside the stationary position and built the curves of ZP vs. focal position. Then we compared the corresponding curves for different pH.

Reflectance UV–visible spectra were collected and converted to Kubelka Munk function using a Perkin-Elmer Lambda 35 scanning spectrometer equipped with an integrating sphere over the spectral range 200–2500 nm (6.2–0.5 eV). $BaSO_4$ powder was applied as a reference. The band gap energies were determined by Shapiro [30] and Tauc [31] methods using Kubelka Munk function.

A three-electrode electrochemical cell was used to characterize the nanoparticle layers via electrochemical impedance spectroscopy (EIS). The cell consists of the FTO glass slides (7 Ω cm−2, Sigma-Aldrich) working electrode, a Pt wire as counter electrode, and an SCE (3M KCl) reference electrode. The working electrodes were fabricated by electrodeposition or drop coating as described earlier.[32] The impedance spectra were recorded on a VMP300, Biologic potentiostat with the Software EC-Lab, between 0.1 Hz and 1 MHz with an amplitude of 25 mV in a 0.1 M $NaClO_4$ electrolyte in the range of pH between 6 and 10 adjusted with NaOH or $HClO_4$. For each applied potential an equilibration time of 10 min was applied to reach a steady-state current before the impedance measurement.

2.3. Catalytic tests.

A batch slurry photoreactor was used in all experiments. A weighted amount of powder catalyst or of methanol slurry containing from 0.6 to 90 mg of the catalyst was added to 30 ml of pure methanol or water-methanol reaction mixture. A 125 W high-pressure mercury lamp was applied with the window of 21 cm^2 area. A quartz optical window and a Pyrex window cutting light below 300 nm were positioned between the lamp and the reaction mixture. The photoreactor had gas inlet and outlet used to purge the system with argon before the reaction and to sample the gases during the reaction. The gases were analyzed with Agilent 3000A micro gas chromatograph. The volume of (water-) methanol slurry was 30 mL and catalyst

concentration was from 0.02 to 2.5 g L^{-1}. Before the irradiation, the solution was stirred for 10 min and the reactor was purged with Ar flow. PHER rate and methanol conversion were calculated from the integration of chromatographic peaks during the reaction period of 3 h. To check the stability, the experiments were repeated for several times with the same reaction mixture, after refreshing methanol and purge with Ar. The methanol conversion in all experiments was below 0.1 %. No CO_2, CO or other secondary methanol conversion products were detected, in agreement with the literature findings demonstrating that the primary reaction is dehydrogenation to formaldehyde, equation (1) [33,34].

$$CH_3OH \rightarrow CH_2O + H_2 \quad (1)$$

The apparent photonic efficiency (PE) was calculated by dividing the amount of released H_2 by the integrated absorbable photon flux [35]:

$$PE = \frac{r_{H_2}}{\Phi_{phot}} \quad (2)$$

where r_{H2} is the hydrogen formation rate and Φ_{phot} is the absorbable photon flux. The UV lamp is polychromatic (Fig. S1), the flux of absorbable photons Φ_{phot} is 1370 µmol/h.

3. Results and discussion.

3.1. Properties of the IF-MoS_2 materials

The IF-MoS_2 size-tuned sulfide particles were obtained from solid–gas reaction of Scheelites $AMoO_4$ (A=Ca, Sr, Ba) with H_2S and CCl_4 vapor. The reaction produces MoS_2 and soluble ACl_2 chlorides, which are removed by washing [36]. The properties of size-tuned IF-MoS_2 including characterizations with multiple physical techniques (XRD, XPS, Raman, TPR, etc.) were discussed in detail in ref. [25]. For the present study, several preparations were selected that give weakly agglomerated and isotropic particles with the mean radius 18, 35 and 71 nm, prepared at 450 or 750 °C (Table S1, Fig. S2). The amount of residual slabs edges on the surface of IF particles depends on the preparation temperature but not on the particle size. On the other hand, the IF-MoS_2 particle size is determined by the particle size of the Scheelite precursor. Therefore the particle size and the amount of surface defects were controlled independently. The major part of experiments was focused on the IF-MoS_2 with sizes at the extremities of the series ("small", 18 nm and "large", 71 nm) treated at the two most distant

temperatures ("low", 450 °C and "high", 750 °C). Note that already at the lowest preparation temperature (450 °C) the residual amount of slabs edges exposed by IF-MoS_2 is much lower that the corresponding value for the disordered ATM-MoS_2 [37]. In most experiments four IF-MoS_2 solids as described were associated in different ratios with anatase PC500 TiO_2. Intermediate 35-nm radius IF-MoS_2 particles, treatment temperatures intermediate between 450° and 750° as well as different titanias including TiO_2 rutile nanorods and Degussa P25 TiO_2 were also applied when necessary to better illustrate the observed effects.

3.2. Suspensions and composite catalysts

Even if in the PHER tests the IF-MoS_2 and TiO_2 particles were usually associated only *in situ* in the catalytic slurry, in the further discussion we consider these systems as composite catalysts IF-MoS_2/TiO_2 with variable Mo loading. Prior to being associated, IF-MoS_2 and TiO_2 were suspended separately in water or water-methanol mixtures and the suspensions were characterized with DLS and Zetametry.

Freshly sulfided IF-MoS_2 solids unloaded from the sulfidation reactor and washed with water upon stirring, remained compact and could be easily decanted. However even after gentle sonication, dark aqueous dispersions of IF-MoS_2 were formed, stable for a prolonged time (at least for weeks). The suspensions stability depended on the particle size, smaller particles being expectedly more stable, Fig S3. The hydrodynamic particle size was determined by DLS. The DLS curves attest narrow size distributions and good correlation between primary TEM particle size and the DLS size (Fig. S4). However the DLS hydrodynamic size is systematically larger than the corresponding mean TEM values. Moreover DLS shows slight agglomeration of IF-MoS_2 particles (Fig. S4). Even if their TEM sizes are similar [25], broader and more skewed to higher size DLS distributions were obtained for the solids prepared at 450 °C, than for 750 °C preparation. It happens probably because the IF-MoS_2-450 solid contains greater amounts of surface functional groups and is more prone to agglomerate. After sonication, DLS shows size stability for at least several hours, whatever the type of IF-MoS_2 particles (Fig. S5).

PC500 TiO_2 contains 5-10 nm size primary particles strongly agglomerated in the suspensions at neutral pH. Both DLS and TEM studies showed porous agglomerates of 200 nm and greater size (Fig. S6, S7, S8). TiO_2 agglomerate size depends on the slurry concentration and in particular on the suspension pH [38]. Detailed investigation of such effects is beyond the scope of this work. Under the conditions applied, PC500 TiO_2 exists in suspensions as 200-300 nm size agglomerates (which count, by order of magnitude, ~10^4 primary particles in one

agglomerate). After addition of IF-MoS_2 to TiO_2, DLS shows only large agglomerates of TiO_2 phase. Even for the highest loadings of IF-MoS_2 in the composite materials, no sizes characteristic for the IF-MoS_2 particles were seen in the DLS distributions (Fig S8). Inclusion of sulfide particles into the larger PC500 titania agglomerates is obvious as the composite slurries settle down with formation of colored precipitates and colorless surnatant liquids. Therefore otherwise stable suspensions of sole IF-MoS_2 are destroyed by contact with titania PC500 agglomerates.

Stability of suspensions and particles charge was estimated from Zeta potential measurements. Depending on the size and on the chemical nature of suspended particles a Zeta potential of 20-30 mV is generally required to achieve reasonably stable dispersions. Figure 1 presents Zeta potential for different TiO_2 powders and two IF-MoS_2 solids, measured in 1:1 water-methanol mixture containing 0.001M KNO_3. TiO_2 materials show similar behavior with IEP at 6.0 for rutile nanorods, 6.1 for PC500 and 6.8 for P25. Two IF-MoS_2 samples show similar behavior with IEP < 2.5. For the two extreme cases of smaller particles heated at relatively low temperature (IF-MoS_2-18-450) and large particles heated at high temperature (IF-MoS_2-71-750), Zeta potential is negative in the whole range of pH > 2.5. Lower electrophoretic mobility for IF-MoS_2-71-750 is probably related to lower surface area and decreased amount of surface functional groups. At neutral pH applied for the catalytic tests, TiO_2 suspensions are not stable. By contrast IF-MoS_2 samples have a net negative charge in these conditions. Though the values of Zeta potential are moderate, low amount of functional groups on the surface of IF-MoS_2 probably allows stabilization even at these values. At neural pH titania particles have a weak positive zeta-potential, whereas IF-MoS_2 particles are negatively charged. Therefore electrostatic attraction between titania and IF-MoS_2 particles should exist, explaining observed adhesion of IF-MoS_2 on the exterior of PC500 agglomerates.

After catalytic tests the solids were separated from the slurries by decantation, dried in inert and characterized by XRD, UV-visible reflectance spectroscopy and TEM, in order to access possible interactions between IF-MoS_2 and TiO_2 and eventual changes in the structure of the co-catalyst. As there appeared to be essentially no difference of the observed properties before and after PHER tests, we present post-mortem characterizations for the most active composites containing IF-MoS_2 and PC500 oxide.

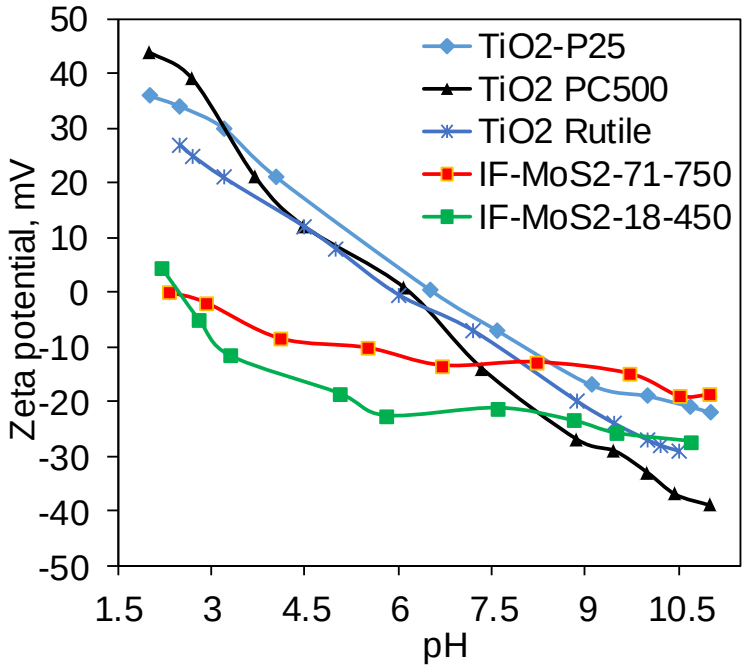

Fig. 1 Zeta potential of TiO_2 powders and two IF-MoS_2 samples as a function of pH in 10^{-3} M KNO_3 in 50 % vol. water-methanol mixture.

XRD patterns are not diagnostic of any interaction and expectedly show mechanical mixtures of MoS_2 and TiO_2 (Fig. S9). In the UV-visible spectra of composite catalysts after PHER test, the regions of absorption due to TiO_2 and MoS_2 are well distinguishable and weakly overlapping. Whatever the MoS_2 type and loading, the same features were observed. For MoS_2, beside the main ill-resolved peak at 450 nm, two characteristic lines at 612 and 674 nm are seen [39,40]. These lines do not change position and their intensity changes in step with the amount of MoS_2 in the composite. Closed-shell IF morphology does not modify the UV-vis absorption spectra: indeed, a mechanical mixture of TiO_2 with ATM –MoS_2 shows the same features of the UV-vis spectrum as IF-MoS_2 (Fig. 2). The band gap of TiO_2 remains at 3.24(4) eV in all samples, suggesting that the electronic properties of titania are not significantly modified. TEM images of the solids after catalytic test show isolated IF particles as well as agglomerates of several IF particles adhered to TiO_2 agglomerates (Fig. 3a-d). The IF-MoS_2 particles preserve their closed-shell morphology. The contact between MoS_2 and TiO_2 occurs via the basal planes of sulfide (Fig 3e, f). As far as TEM of dried samples represents the solid morphology in the slurry, it can be concluded that the IF-MoS_2 particles are located at the exterior of titania agglomerates.

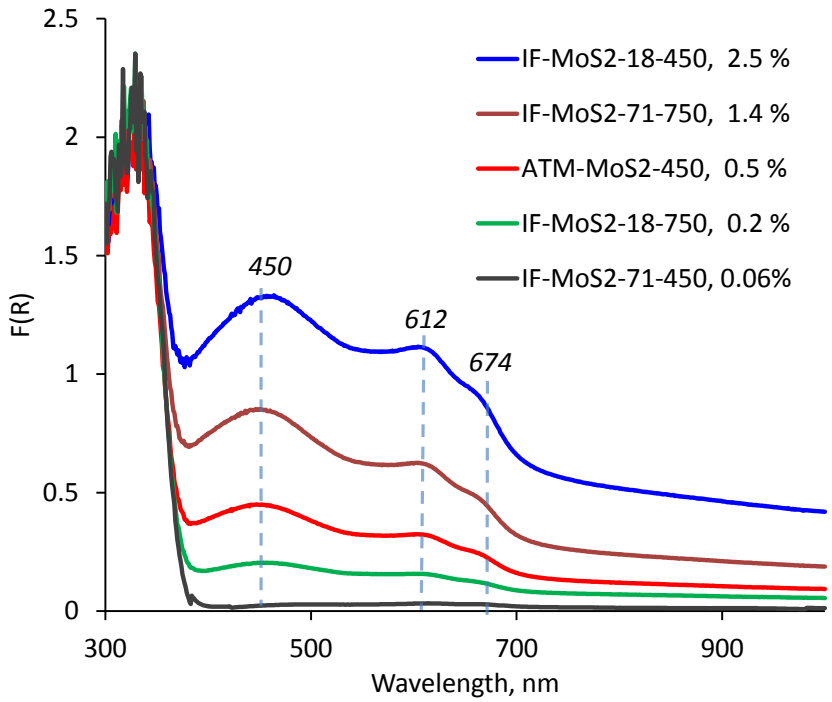

Fig. 2. UV-Visible spectra of TiO_2-MoS_2 composite catalysts after the PHER test. The mixtures were prepared with different MoS_2 loading indicated in legends (% wt.).

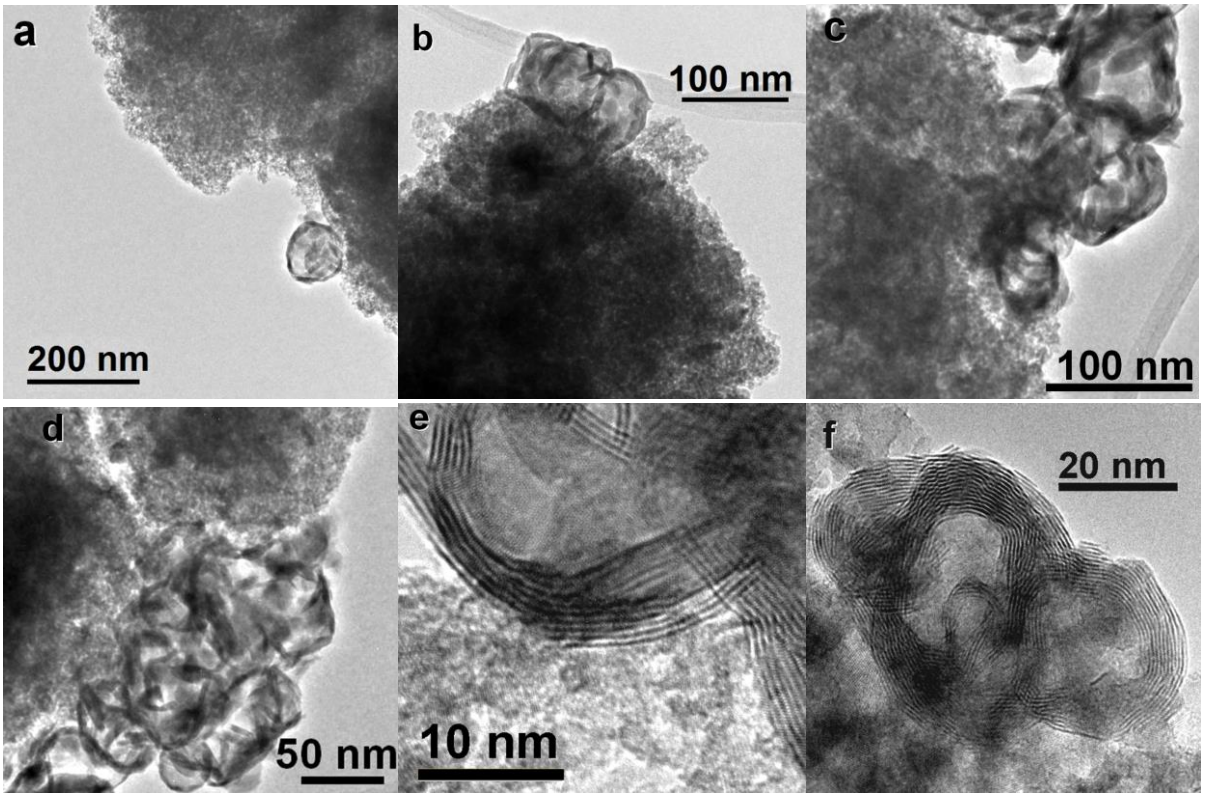

Fig. 3. TEM images of composite materials recovered after catalytic test (according to co-catalyst used, all on PC500 TiO_2): IF-MoS_2-71-450 (a), IF-MoS_2-71-750 (b), IF-MoS_2-35-750 (c), IF-MoS_2-35-450 (d), IF-MoS_2-18-450 (e) IF-MoS_2-35-750 (f).

3. 3. Photocatalytic hydrogen production activity.

PHER rate was systematically studied as a function of several parameters. Firstly we focused on the PHER rate versus the IF-MoS_2 properties, the slurry concentration and the relative amount of IF-MoS_2 vs. TiO_2. Other factors were also studied including water – methanol ratio and the nature of TiO_2. The catalysts were compared with Pt/TiO_2 reference and with similar slurries containing non-IF molybdenum sulfide, generated from the decomposition of ammonium thiomolybdate (ATM-MoS_2). PHER activity of impregnated and deposited 0.8 wt. %. MoS_2/TiO_2 prepared according to ref. [19] was measured in a wide range of slurry concentrations and compared with the systems under study to unravel the influence of the preparation technique and of the MoS_2 morphology.

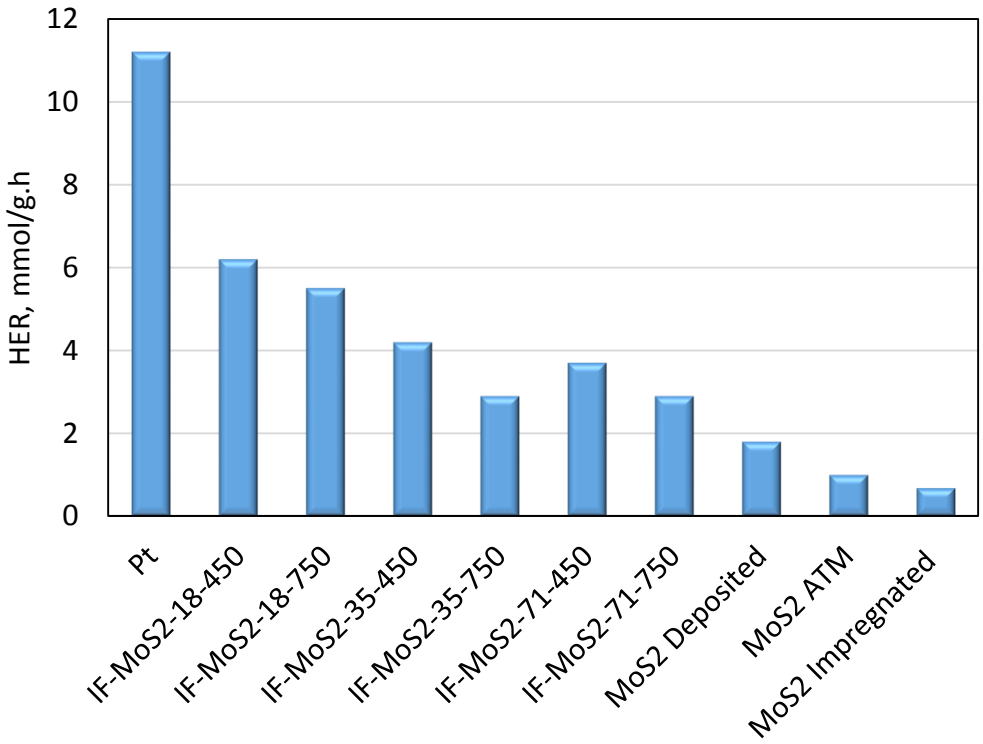

Fig. 4. Specific PHER rate as a function of preparation technique for the MoS_2/TiO_2 catalysts, as compared with Pt/TiO_2 reference (maximal observed value is given for each preparation type).

The highest observed values of specific PHER rate for the MoS_2/TiO_2 materials prepared by different techniques and for Pt/TiO_2 reference are shown in Fig. 4. Specific PHER activity as a function of slurry concentration for three different IF sizes is depicted in Fig. 5 for the loading corresponding to 0.8 %wt. IF-MoS_2/TiO_2. Activity as a function of IF-MoS_2 loading for selected samples is presented in Fig 6. Additional data on the activity of these systems are reported in the SI (Fig S10-S12).

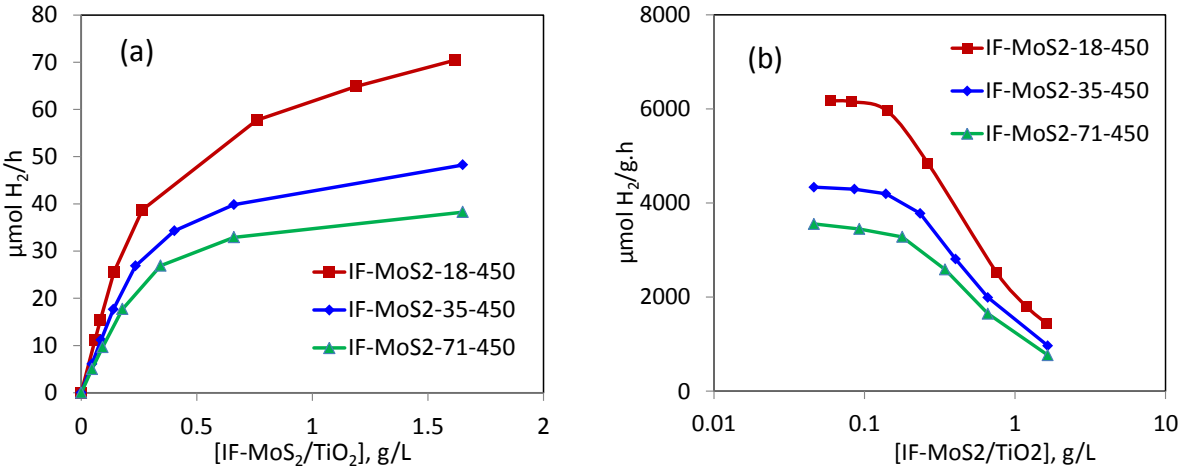

Fig. 5 Total (a) and specific (b) PHER rate as a function of slurry concentration for different IF-MoS_2 particle sizes. All IF-MoS_2 samples were prepared at 450 °C. MoS_2 loading is 0.8 % wt.

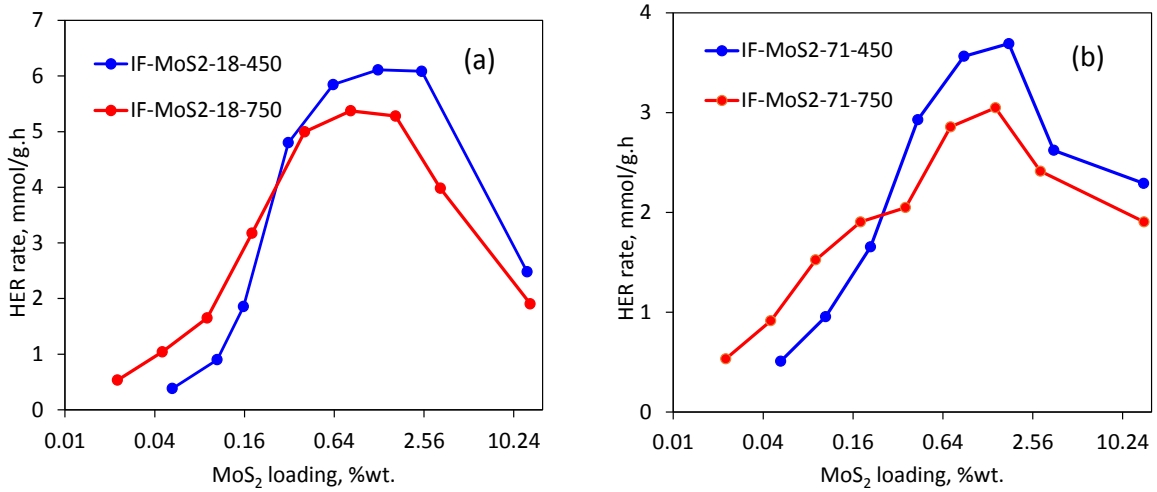

Fig . 6 Specific PHER rate as a function of MoS_2 (%wt.) loading on PC500 TiO_2 for IF-MoS_2-18 (a) and IF-MoS_2-71 co-catalysts (b), prepared at 450 and 750 °C. Slurry concentration is 0.1 g/L.

As follows from comparison with the (re-calculated) literature values (Table S2, refs [16, 41, 44, 46, 47, 48]), the IF-MoS_2 /TiO_2 system is among the best reported PHER catalysts of this type. Note however, that direct comparison with the literature is difficult because even for similar MoS_2/TiO_2 systems, different conditions are used in different laboratories, such as light source and reactor geometry. More straightforward idea of the catalysts performance and ranking might be given by comparison with benchmark references. In comparison with 0.5% Pt/TiO_2, the best IF-MoS_2-450 co-catalyst gives nearly 50 % PHER rate (Fig. 4, Fig. S11). On the other hand, IF-MoS_2 showed greater PHER activity than all MoS_2-containing references tested in this work. Prepared using a similar procedure of mechanical mixing, non–IF bulk ATM-MoS_2 in a slurry with PC500 showed significantly lower activity (Fig. 4). Previously

studied impregnated and deposited MoS_2-TiO_2 catalysts are even less performant at equal Mo loading and slurry concentrations. Remarkably, impregnated catalyst with the highest MoS_2 dispersion and the most exposed slabs edges was the least active. PHER activity of the individual components has been also checked. No hydrogen production occurs in the presence of sole IF-MoS_2 in pure methanol or water-methanol mixture. Bare PC500 titania has measurable PHER activity (~35 μmol/g.1.h for 1.5g/L slurry), which is two orders of magnitude lesser than for the best composite catalysts.

The nature of TiO_2 appears to be important. PC500 solid gives significantly higher PHER rates than P25 titania. Rutile nanorods show inferior PHER rates which might be due to the intrinsic advantage of anatase over rutile (Fig. S11).

The IF-MoS_2 particle size has a clear impact on the observed PHER activity. Smaller IF-18 particles systematically give higher PHER rates than larger ones, in the sequence IF-18 > IF-35 ≥ IF-71 (Fig 5, 6). The observed effect of IF particle size on the HER rate (nearly 50 % relative value) is by far lesser than the variation of the specific surface area from IF-MoS_2-18 to IF-MoS_2-71, which is threefold (Table S1). The existing moderate difference might be related to better interaction between MoS_2 and TiO_2 for the smaller particles and other fine details of the mechanism. It should be emphasized again, that even "small" IF-MoS_2 particles are very large as compared with those in the impregnated and deposited references.

The observed PHER rate as a function of MoS_2 loading has maximal values in the range of loadings 0.5-2 wt. %, depending on the IF-MoS_2 sample (Fig. 6). At lower co-catalyst loadings expected decrease of activity occurs. Whatever the mechanism of co-catalyst action, some lowest amount of co-catalyst obviously exists, necessary to harvest the photo generated electrons. Expectedly, for larger particles higher loadings are necessary to achieve this limit. Therefore the decline of the PHER rate began at higher loadings for the IF-71-MoS_2 solids than for IF-18-MoS_2 ones (Fig. 6). On the high loading side, for all co-catalysts, the PHER rate decreased above 2% wt. (Fig. 6). Such decrease might be attributed to non-productive light absorption by MoS_2 or to electron-hole recombination promoted by the co-catalyst (vide infra). In the region of optimal mass loadings, the PHER rate has a plateau or a smooth maximum.

The influence of the IF-MoS_2 preparation temperature is illustrated in Figure 6. For both small and large particles, the increase of the preparation temperature from 450°C to 750 °C leads to a decrease of PHER rates, apparently because of the decrease of defects and edges concentration upon sulfide annealing. Again, the magnitude of the effect on PHER is moderate and by far lesser than the variation of the number of residual slabs edges. As determined in the previous work [25] the amount of residual edges decreased by orders of magnitude from 450 to 750 °C.

This finding suggests that while edges and defects are obviously necessary for the PHER to occur, reaction on the surface of MoS_2 is not the rate-limiting step for the whole process (unlikely to heterogeneous catalysis and electrochemical HER).

The effect of water – methanol mixtures composition was studied for several selected catalysts (Fig. 7). The activity had a smooth maximum at 10-20 % vol. H_2O then slowly decreased with the amount of water, up to 90% H_2O. At low methanol concentrations, a sharp decrease was observed. In pure water only a small residual activity was detected for a short time, but overall water splitting was extinct after 1-2h.

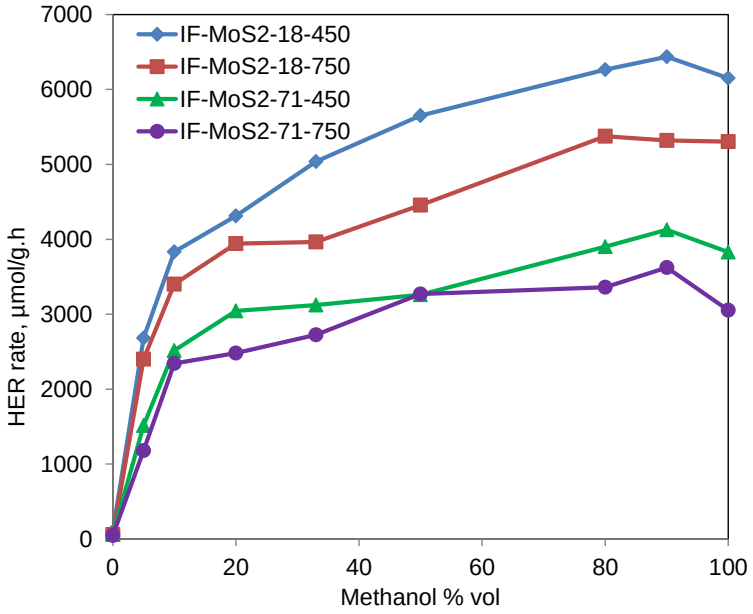

Figure 7 Specific HER rate as a function of water–methanol mixture composition.

In summary, highly active composite catalysts were obtained, more performant than the reference catalysts of the same type. Surprisingly, mechanically mixed in solution and poorly dispersed IF-MoS_2 shows much greater activity than finely dispersed MoS_2 in an intimate contact with titania surface (as it is present in the deposited and impregnated samples). Moreover IF-MoS_2 systems are by far more stable than highly dispersed MoS_2 which is slowly but steadily oxidized towards soluble Mo blues [42]. The influence of the properties of IF-MoS_2 nanoparticles on the PHER rate appears non-negligible but rather moderate. Provided that IF-MoS_2 is dispersed in water-methanol slurry with PC500 titania in a 0.5-2 % wt. amount, high PHER rates are always obtained. By contrast, the nature of TiO_2 and the preparation technique of the MoS_2 co-catalyst (i.e. MoS_2 morphology and its interaction with TiO_2) play a crucial role and may modify the PHER rate by an order of magnitude.

3.4. Demonstration of the trapped electrons transfer.

Liquid-phase PHER is a complex multistep process which includes light absorption, carriers transport, chemical reaction, desorption and diffusion of the products. Depending on the conditions, each step can become limiting for the whole PHER process. In an optimal photocatalyst the rate limiting step is supposed to be that of the light delivery, i.e. all photons are absorbed and used to produce H_2. The current efforts on PHER catalysts design are in a great extent inspired by the field of photoelectrochemical devices. It is often (implicitly) supposed that the bottleneck of the overall PHER process is related to the reaction on the co-catalyst or to the interface transfer of charge carriers. By consequence the best PHER performance is striven to be achieved by optimizing these properties. In particular, good contact and easy charge transfer between MoS_2 and TiO_2 is considered mandatory for high PHER performance [43, 44]. To this aim, MoS_2-TiO_2 epitaxy, the use of metallic exfoliated MoS_2 phase [45] or doping with conducting materials [46, 47] were applied. At the same time, TiO_2 is modified with respect of morphology and crystalline facets exposure [48, 49] whereas the MoS_2 co-catalysts are optimized to expose the highest possible amount of active edges, [50, 51] by analogy with the MoS_2-based electrochemical HER catalysts [52].

However, as demonstrated in the previous section, highly active catalysts could be obtained by mechanical mixing of TiO_2 and IF-MoS_2 suspensions assisted with a gentle ultrasound treatment. Taking into account spherical shape and relative inertness of IF-MoS_2, the contact between MoS_2 and TiO_2 is by far lesser than in the impregnated and deposited references. Moreover, the surface of IF-MoS_2 exposes mostly inert basal planes, albeit curved. The catalysts under study are quite poorly dispersed as compared with the impregnated counterparts. Even the smallest particles in the IF-MoS_2-18 are by three orders of magnitude more massive than 4-5 nm MoS_2 slabs in the supported MoS_2/TiO_2. Moreover, as shows TEM study, the MoS_2 particles are localized at the exterior of large TiO_2 agglomerates, never penetrating inside them. With respect to the existing literature the observed results seem highly counterintuitive.
In addition to the results of the section 3.2, we observed that sonication even for prolonged periods (up to 4h) that would improve the components mixing, does not significantly modify the PHER rates (Fig. S13). Post mortem inspection of the best composite catalysts revealed that a considerable part of TiO_2 agglomerates do not contain adhered IF-MoS_2 particles, as exemplified in Fig S7. Therefore transfer of active species between TiO_2 and IF-MoS_2 probably occurs upon collisions in the slurry. Taking into account large size of TiO_2 agglomerates and

considerable part of bare TiO_2 in the optimal catalysts, for such an interaction to be efficient, the transferred species should be long – live and highly mobile, in order to survive between the collisions and to travel along the distances of 200-300 nm (typical size of TiO_2 agglomerates.

It is well-known that photo generated electrons are highly mobile in the polycrystalline TiO_2 agglomerates. Indeed, the mobility of electrons in polycrystalline TiO_2 specimens was shown to extend up to the micrometer scale, being by several orders larger than the mobility of holes [53, 54]. On the other hand, long-live species are described in the literature known as trapped electrons (TE), alternatively called accumulated or stored electrons. They appear upon UV illumination of bare titania in the presence of hole scavengers (e.g. in alcohol medium) and cause its blue coloration as TE are apparently located at a metal ion (Ti^{3+} species) with an oxygen vacancy [55,56,57]. The possibility of using TE to reduce molecular species has been demonstrated earlier in organics hydrogenation [58,59] or nitrogen fixation [60].

Our experimental observations suggest that TE are transferred from the TiO_2 particles to IF-MoS_2, where they generate molecular hydrogen. To prove this, a series of experiments was carried out in which accumulated electrons were used to produce hydrogen from methanol in the dark. In such experiments, bare titania was illuminated for 1h, then light was switched off and a calculated amount of sulfide suspension (1% IF-MoS_2 by weight on TiO_2) was injected into a blue TiO_2 slurry via a septum. Rapid release of H_2 was observed in all cases, which ended within the first 10-20 minutes after the injection (Fig. 8a). The amount of TE has been estimated from the limiting amount of hydrogen released in the dark. It has the values of 30-50 μmol/g, in the same range as the amounts of stored electrons determined from photoacoustic spectroscopy and reactions with organics [53-55].

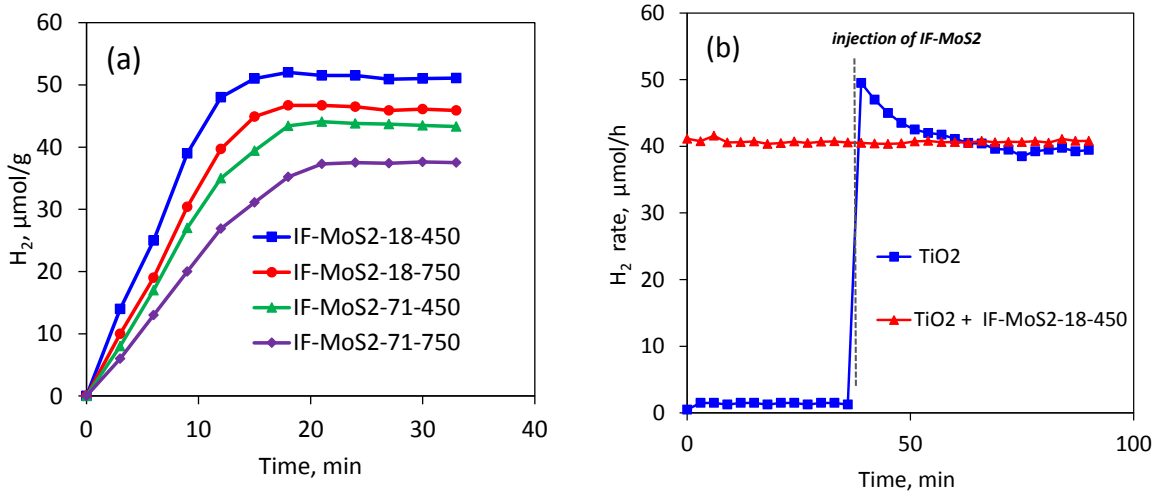

Fig. 8 H_2 release in the dark, after 1 h UV irradiation of bare TiO_2, followed by injection of IF – MoS_2 suspensions (a) and effect of IF-MoS_2 injection into a continuously illuminated titania slurry (b).

In an ideal case, the same amount of H_2 should be released due to reaction of accumulated electrons after the same illumination time, whatever the co-catalyst. However as the TE have limited lifetime and traces of oxygen are unavoidable in the system, the co-catalysts having slower PHER rates equally show lower amounts of H_2 released in the dark (Fig.8). Whatever with this limiting amount, the results of dark experiment shown in Fig 8a give a direct evidence that TE are transferred from the titania to the sulfide and then produce hydrogen.

In order to see how quickly the interaction is established and the steady state PHER rate is attained, an aliquot of IF-MoS_2 suspension was injected into the slurry of bare TiO_2 upon constant illumination. An abrupt PHER rate jump occurs immediately after the injection (Fig. 8b). During the first 20 min after the injection of IF-MoS_2 the PHER rate was greater than in the steady state experiment, probably due to the release of the excess of accumulated electrons. Then it settles down to the level of steady state (Fig. 7b). As the mixed suspension was not sonicated after injection, it proves that the ultrasound treatment is not necessary to obtain highly active catalysts.

The PHER rates reported up to this point refer to the catalysts produced by combining IF-MoS_2 and TiO_2 directly in the liquid phase. It could be questioned however if the composite catalysts at stake have a potential to be further improved by increasing connectivity between the components. Such improvement could be achieved by thermal treatment of the solid materials. The composite catalysts were isolated as powders and treated in Ar or H_2 flow at different temperatures in the range 400-750 °C. Figure S14 represents variation of PHER rate vs temperature for the catalyst 0.8% IF-MoS_2-450. A slight increase of activity was observed after heating or reduction at 350- 450 °C. Then the PHER activity decreased with pre-heating temperature, more rapidly in H_2 than in Ar. A slight increase of the PHER rate might be explained by the increase of titania connectivity, in lines with the work by Kowalska and coll, who reported an improvement of interparticle electron transfer between thermally agglomerated TiO_2 particles [61]. This result is also in good agreement with the work by Haruta and coll, reporting an increase of PHER at low Pt loading on agglomerated titania [62]. However this effect (about 10-15% relative PHER rate increase) might be fully explained by better connectivity of TiO_2 agglomerates as observed in the previous works, without evoking MoS_2-TiO_2 interactions. The PHER rate dropped upon further increase of the treatment temperature above 400 °C, probably because the decrease of specific surface area overweighs the improvement of connectivity (Fig. S14).

3.5. Flat band potential measurements

To get a better insight into the transfer of accumulated electrons, the energy bands alignment in the corresponding solids is considered in this section. Both TiO_2 and 2H-MoS_2 are semiconductors. The band gap Eg of MoS_2 depends on the material properties (particle size, layers stacking, doping) but is comprised between 1.2 and 1.9 eV, i.e. is always considerably lesser than 3.2 eV band gap of anatase. The VB edge of MoS_2 containing a major contribution of S 3p orbitals is commonly recognized to be significantly higher than VB edge of TiO_2, which has mostly O 2p character [63]. However as concerns the CB bands alignment, there is some controversy in the literature.

In a majority of works using electrochemical methods or high-vacuum XPS (UPS) techniques as well as DFT calculations [64, 65, 66, 67, 68, 69], the energy position of TiO_2 CB bottom is found to be superior (more negative) than the bottom of CB in MoS_2, in agreement with observed electrons transfer from TiO_2 to MoS_2. However, several recent works place the bottom CB of MoS_2 above that of TiO_2 and advocate mechanistic schemes in which TiO_2 plays the role of electrons acceptor and hosts the reduction sites, whereas MoS_2 donates photo generated electrons and is responsible for the oxidation half-reaction [70, 71, 72, 73]. Unraveling this controversy would probably deserve a dedicated investigation, far beyond the aims of this work. However the CB alignment for the materials under study was checked under the conditions close to those of the PHER experiment by means of flat band potential (U_{FB}) electrochemical measurements. The flat-band potentials of the powders at various pH were evaluated using the Mott–Schottky method [74], based on eq (3):

$$\frac{1}{C^2} = \frac{2}{\varepsilon\varepsilon_0 e N_D}\left(V - U_{FB} - \frac{k_B T}{e}\right) \quad (3)$$

Where C is the normalized interfacial capacitance, ε and ε_0 are the dielectric constant of the semiconductor and vacuum permittivity, N_D is the charges density, V is the voltage, k_B is Boltzmann's constant, T is the temperature, e is the electron charge.

Nyquist EIS plots and Mott-Schottky (MS) plots for TiO_2, IF-MoS_2 and a composite material containing 0.8 % IF-MoS_2 are depicted in Fig. 9. The EIS curves (Fig. 9a) provide general information on the electrodes behavior, complementary to the MS measurements which are carried out only at relatively high frequencies. In the frequency range 100 KHz -0.1Hz, Randles circuit describes the response of the systems (Fig 9a, inset): R_S represents the series resistance from the electrodes, electrolyte and contacts; R_{CT} describes the charge transfer resistance at the electrolyte–electrode interface. Constant phase element (CPE) describes capacitance of the

electrode and deposited material (Fig. 9a, inset). Compared with the pure FTO glass, the charge transfer resistance R_{CT} of the TiO_2-coated FTO electrode is higher due to partial blocking of the conducting FTO glass by the dielectric TiO_2 nanoparticles. Composite IF-MoS_2/TiO_2 material shows behavior close to that of pure TiO_2 as only a small volume fraction and no percolation network of MoS_2 is created. Deposit of IF-MoS_2 shows decreased charge transfer resistance due to considerable conductivity of molybdenum sulfide (Fig. 9a).

The positive slopes of the MS plots (Fig. 9b) confirm that both TiO_2 and IF-MoS_2 are n-type semiconductor. The U_{FB} obtained from the MS plots could be approximately regarded as equal to the bottom of CB energy. Despite its simplicity, for deposited powders electrochemical FB determination technique has several pitfalls, related, among others, to the influence of substrate –electrolyte interface [75,76]. The MS plots of pure FTO and deposits were therefore compared. In the zone -0.6-1.0 V vs. SCE, the C^{-2} values of pure FTO are several times higher (capacitance lower) than for the deposits (Fig. S16). In this region the MS curves are related to the properties of the powers under study and not to the electrolyte-FTO substrate interface. Therefore, despite possible capacitive contributions from the electrode–solution interface, reliable values of U_{FB} could be obtained. In the region -0.4-0 V vs. SCE, FTO contribution is important with U_{FB} being in the range −0.4-0.6 V, depending on pH. At the potentials below −0.5-0.7 V vs. SCE, a strong increase of the capacitance is observed because of contribution of the deposited nanopowders. Convergence of U_{FB} measured at different frequencies has been checked as well (Fig. S17). Taking into account different sources of systematic errors the measured U_{FB} values have accuracy within at least 0.05 V range. The measured values of U_{FB} for TiO_2 showed Nernstian dependence, i.e. shifted by 59 mV/pH unit over the pH range of 6–9. Composite IF-MoS_2/TiO_2 material shows behavior similar to that of pure TiO_2. By contrast pure IF-MoS_2 deposited on FTO has lower U_{FB} in the whole range of measurement and does not show Nernstian behavior, but changes with a coefficient near 20 mV per pH unit (Fig. 9c). This observation agrees with earlier literature. Many non-oxide (sulfides) systems show no clear pH dependence of the U_{FB} but do show a Nernstian type dependence on the concentration of potential determining ion. For example, in the CdS sulfide, U_{FB} depends on the S^{-2} concentration [77]. It has been observed previously that MoS_2 does not show Nerstian behavior vs. medium pH [78].

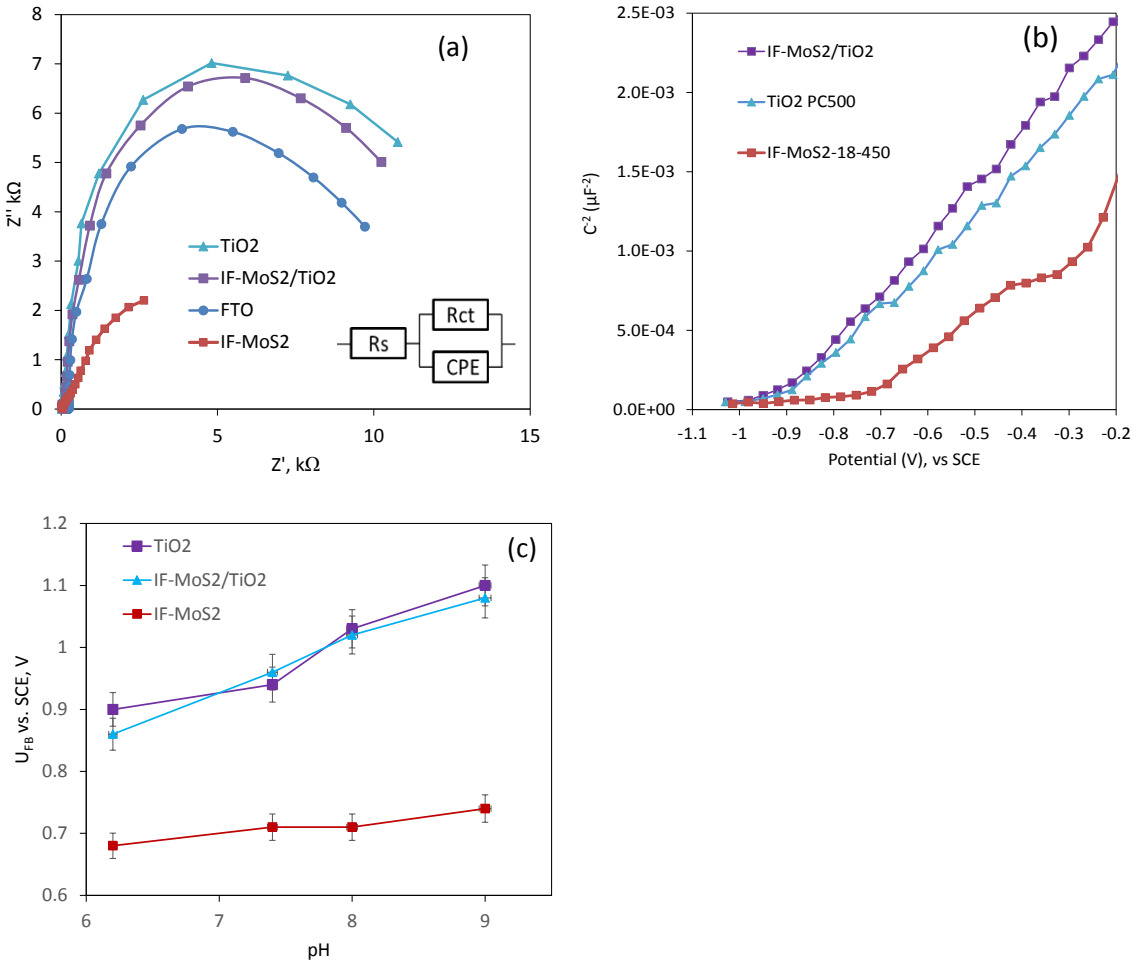

Fig. 9 EIS curves (a) Mott-Shottky plots (b) and pH dependence of U_{FB} (c) for pure TiO_2 PC500, composite material containing 0.8 %wt. IF-MoS_2-18-450 and pure IF-MoS_2-18-450.

Nernstian behavior of U_{FB} observed for TiO_2 and its absence for IF-MoS_2 could be correlated with Zeta-potential measurements reported in the section 3.2. Indeed, the surface charge for TiO_2 strongly depends on the applied pH, whereas MoS_2 particles have weak negative charge in the whole range of pH studied, which much lesser slope. The literature discrepancies on the band alignment according to flat band potential measurements could be therefore tentatively explained by different conditions (pH, ionic species) applied for the measurements in different cases.

Overall, it follows from the U_{FB} measurements that CB bottom of IF-MoS_2 is located slightly below (less negative) than that of TiO_2. Therefore, both CB and VB edges of MoS_2 lie inside the forbidden zone of TiO_2 and transfer of both electrons and holes from the oxide to the sulfide should be favorable (Fig. 10a).

Note in addition that charge separation schemes in which molecular oxygen is formed on MoS_2 seem hardly compatible with known corrosion of this sulfide which is easily oxidized with

ambient oxygen [42]. It seems more probable that MoS_2 (and in particular its chemically reactive edges) would rather be oxidized by active species issued from the evolution of holes than produce molecular O_2.

3.5 Mechanistic considerations

The TE transfer as evidenced in the previous section coherently explains most of the experimental observations. Thus, greater activity observed for PC500 could be explained by higher surface area and greater amounts of the accumulated electrons than on P25. On the other hand, well-known longer lifetimes of TE on anatase as compared with rutile explain the observed strong advantage of anatase samples over rutile nanorods.

However, despite the evidence that PHER mechanism involves the TE transfer, it remains necessary to explain why high dispersion of MoS_2 on TiO_2 in the impregnated and deposited samples leads to lower activity than that observed for poorly dispersed IF-MoS_2 (Fig. 4). In other words, if the TE transfer occurs between TiO_2 and IF-MoS_2, then why does not it occur with the same or even greater efficiency when supported MoS_2 is finely dispersed and tightly interacting with TiO_2? Obviously, the amount of defects and slabs edges of the MoS_2 co-catalyst is not a key parameter, as in this case impregnated and deposited systems would be much more active. The only possibility to explain high PHER rates for the systems at stake is a lesser electron – hole recombination. As pointed by Ohtani, charge separation and recombination arguments are often abusively applied to explain the observed activity. This is in part related to the difficulty of recombination measurements [79]. Here we present a mechanistic scheme which with minimal assumptions qualitatively demonstrates how optimal PHER performance vs. the co-catalyst loading might be achieved. To demonstrate that, the only required assumption is that recombination on the co-catalyst is possible. The details of the mechanistic scheme (e.g. the exact values of rate constants) require further study with physical techniques such as, for example, photoacoustic spectroscopy [80]. The main point of the model is to explain the existence of a maximum of PHER activity as a function of the amount of MoS_2 co-catalyst in the presence of electron-hole recombination on it.

In the following we write down the mechanistic rate steps that involve the intermediate species existing in the solid (electrons and holes). Stable chemical species whose concentrations are supposed to be constant are put in the equations into curled brackets. The concentrations of these species do not explicitly participate in the differential rate equations but enter into the respective rate constants. Thus, concentrations of electrons [e] and holes [h] in titania are

supposed to be small with respect to the amount {TiO_2} of titania sites remaining unaffected by light. Similarly, the concentration of methanol {CH_3OH} is supposed to be constant throughout the reaction. Complex mechanisms of surface chemical reactions of protons reduction and methanol oxidation which in general follow Langmuir- Hinshelwood type kinetics, (as considered e.g. refs [34, 81]) are not considered here, as the conversions in all experiments are very low (< 0.1%). Therefore the rates for these complex reactions are just formally embedded within the respective constants.

Photogenerated electron-hole pairs in TiO_2 are produced at a constant rate (k1) but in the absence of chemical scavengers may rapidly recombine (k2):

{Light} + {TiO_2} => e + h (k1)

e + h => {phonons} (k2)

The photo generated electrons in titania [e] may be either transferred to the MoS_2 co-catalyst where they form active intermediate species designated [eMo] (k3) or they may reduce protons to hydrogen directly on TiO_2, leading to small but measurable activity of bare titania (k4):

e + {MoS_2} => eMo (k3)

e + {CH_3OH} => {H_2} (k4)

The electrons rapidly move within titania agglomerates. Their transfer towards the co-catalyst occurs after multiple electron hopping events between primary titania nanoparticles. Mesoporous agglomerates of the TiO_2 nanoparticles provide facile interparticle electrons transfer towards the co-catalyst. Such effect, referred as “antenna mechanism” was explained by considering the porous TiO_2 as antenna for the photogenerated electrons, enabling them to reach the TiO_2 surface [82, 83]. Even if [MoS_2] concentration does not explicitly participate in the rate equations, its amount obviously influences the apparent value of k3, which is an essential parameter of the model. Alcohol is known to suppress surface recombination due to holes consumption [84]. The methanol molecules easily diffuse inside the TiO_2 agglomerates and provide efficient holes trapping at hydroxyl surface groups [85, 86].

h + {CH_3OH} => {CH_2O} (k5)

However, the holes can also be transferred to the co-catalyst (k6). Again, similarly to k3, the amount of MoS_2 is implicitly included in the constant k6.

h + {MoS_2} => hMo (k6)

As the transfer of both electrons and holes from TiO_2 to MoS_2 is favorable, MoS_2 can promote their recombination (k7, Fig. 9b).

eMo + hMo => {phonons} (k7)

Finally, the electrons transferred onto MoS_2 evolve on the MoS_2 surface to produce hydrogen (k8, Fig. 9c). As the PHER rates measured in all the experiments are fairly constant, stationary state is attained in all instances (note that we do not make any assumptions about the nature of the rate-limiting step).

$eMo + \{CH_3OH\} \Rightarrow \{H_2\}$ (k8)

As follows from the experimental results, production of hydrogen on bare titania, related to k4 is small with respect to its production on the sulfide, k8. Neglecting for simplicity hydrogen production on TiO_2, the observed steady state PHER rate can be approximated as k8*[eMo].

The rate steps k1- k8 give a simple system of differential equations that depends on four variables [e], [h], [eMo] and [hMo]. Parametric analysis of this system has been carried out in which each constant was varied by several orders of magnitude. Full account of this parametric analysis is out of scope of this work. Here we aim at the qualitative demonstration of possibility for the observed PHER rate to have a maximum as a function of the amount of co-catalyst added. Numeric simulations show that in a wide range of constants k1-k8 steady the state is rapidly attained, in agreement with the experiment (Fig S18). Parametric analysis within the steady state region has been carried out vs. k3 to follow the PHER rate (approximated as k8*[eMo]) as a function of MoS_2 amount. Indeed, the amount of co-catalyst influences k3 and k6 (assuming them equal for the simplicity of parametric analysis). In a wide range of other constants the steady state level of [eMo] vs. k3 is a curve with a maximum (Fig. S19) qualitatively similar to the experimental curves (Fig. 6). Therefore the mechanism k1-k8 is capable to explain on a qualitative level why an excess of a co-catalyst might be detrimental for the PHER rate.

In qualitative terms, when there are too many MoS_2 sites on the surface of titania, electrons and holes mostly recombine on the sulfide instead of being used for the reaction (Fig. 9b). Note that this model does not contain any speculative assumptions on the modified electronic properties, improved separation of charges etc. but is based only on the experimentally proven or physically obvious mechanistic steps. To give a better intuition of the model, the PHER might be considered as a quasi-two–step process. First the holes are rapidly consumed by the alcohol molecules and TE-bearing titania particles are formed; next these titania particles meet IF-MoS_2 co-catalyst, TE hops from TiO_2 on the sulfide and forms hydrogen (Fig 9c). Under continuous illumination conditions this two-step mechanism is an abstraction, because all steps occur simultaneously. However it becomes an exact qualitative description of reality for the experiments using injection of IF-MoS_2 suspensions after illumination of TiO_2 (Section 3.4, Fig. 8).

The examples of such behavior of overall activity vs. the amount of co-catalyst are well described in the literature for different types of co-catalysts, yet not fully understood. Thus, Mills et al attribute the decrease of PHER activity in methanol on Pt and Pd -loaded TiO_2 to the overlapping of surface zones where the particles provide optimal electrons harvesting [87]. The PHER rate is often deemed to be restricted by the relatively high recombination rate of electron–hole pairs [88]. Higher concentrations of the co-catalyst are thought unfavorable because of its own non-productive light absorbance and the possibility for electrons and holes to be recombined on the same co-catalyst sink [89]. The mechanistic scheme k1-k8 considered above shows that the latter condition is alone sufficient to explain the activity loss at high co-catalyst loadings. Note that the behavior observed in the slurries might be qualitatively different from that in the TiO_2-based PEC devices where charges recombination rate is decreased due to an external bias [90,91].

It remains still unexplained why small and tightly contacting MoS_2 particles on the impregnated and deposited catalysts demonstrate lesser PHER efficiency in the whole range of loadings. The formal scheme k1-k8 is useless here, as it does not tackle the properties of MoS_2 as a function of particle size. According to this formal model, impregnated and deposited catalysts should give the same maximum of activity, but at much lesser MoS_2 loadings, which is not the case. At this point we can only suppose that the intrinsic values of the rate constants depend on the MoS_2 size.

This seems to be a specific property of MoS_2 catalysts, as for noble metals (e.g. Pt/TiO_2) high activity was detected even for subnanometric particle size down to several-atom clusters [92]. It can be speculated that smaller MoS_2 have higher CB and the value k3 decreases due to unfavorable electrons transfer. Verification of this hypothesis needs further experimental study. Also, it seems probable that in smaller (3-5 nm) MoS_2 particles the electrons should have shorter lifetimes than in IF-MoS_2. In the formal model that would be translated as lesser k3 and/or as significant reversibility of the transfer with a new constant k-3.

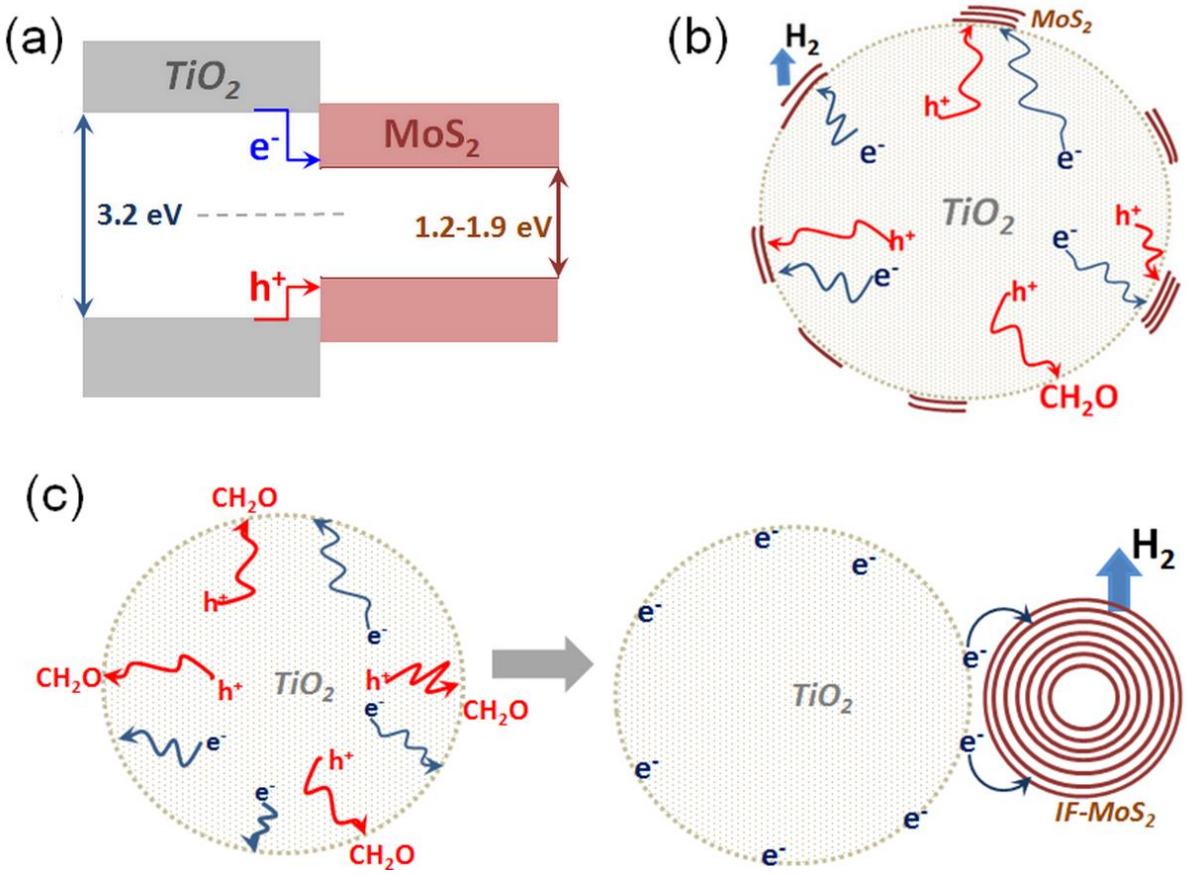

Fig. 9 (a) qualitative sketch of the electronic bands positions in anatase TiO_2 and 2H MoS_2: transfer of both electrons and holes from TiO_2 to MoS_2 is favorable; (b) poor PHER activity on highly dispersed MoS_2 smeared over the surface of TiO_2 is caused by rapid recombination of the $e^- h^+$ pairs on the co-catalyst; (c) two stages of PHER on the TiO_2-IF-MoS_2 system: first the holes rapidly react with alcohol molecules, then accumulated electrons are transferred to MoS_2 where they form H_2.

In the same lines, faster recombination between eMo and hMo (greater k7) would be expected for smaller MoS_2 particles due to higher probability of the electron-hole interaction in a smaller confined space, which would also result in a decrease of observed PHER rate. Variation of MoS_2 electronic properties due to sulfide interaction with the support might be involved as well, but remains beyond the scope of this study.

4. Conclusion

In summary, straightforward evidence is given in the present work that transfer of long-live photogenerated trapped electrons (TE) from TiO_2 agglomerated particles to "inorganic fullerenes" IF-MoS_2 provides an efficient mechanism of photo catalytic hydrogen production (PHER) in water-methanol slurries. The PHER rates are at least as high as in the best systems specially designed to optimize contacts between TiO_2 and MoS_2 phases and to maximize MoS_2

edges exposure. Recently synthesized size –tuned IF-MoS_2 materials available in wide range of preparation temperatures allow a unique possibility to study variations of sulfide particle size and defectness as independent parameters.

Important conclusions could be drawn for the practical design of this type of catalysts. The results of the present study compel us to conclude that the MoS_2 edge concentration is not a critical parameter for the PHER performance in such liquid slurries, because the IF-MoS_2 particles expose low amounts of edges. Moreover, neither a tight interfacial contact between the sulfide co-catalyst and TiO_2 nor fine dispersion of sulfide particles is necessary to have high PHER performance. Indeed, IF-MoS_2 particles are very large as compared with 3-5 nm MoS_2 slabs in the conventional catalysts. The surface of IF-MoS_2 is known to be relatively inert to form mostly van der Vaals non-bonding contacts with other surfaces. Nevertheless this is sufficient to efficiently harvest TE from the exterior of several hundred nm-size TiO_2 agglomerates. It seems that mandatory condition to be met for high PHER rate is to protect the generated TE from being non-productively consumed (recombined with holes). Provided that TE have a sufficiently long lifetime, they are efficiently harvested by IF-MoS_2. Another important property is excellent dispersibility of IF-MoS_2 in the slurries and stability of its colloidal suspensions in water and water-methanol mixtures, first reported here. This allows nanoscale homogeneous mixing of TiO_2 with the sulfide co-catalyst.

These findings open a new prospective for the catalysts design. Indeed, since the PHER co-catalyst can be localized in the suspension outside the TiO_2 agglomerates and still efficiently harvest the photo generated charges, new ways could be foreseen toward space-resolved water splitting systems with oxidation and reduction functions separated at the nanoscale. The preparation procedure is extremely soft as it involves mechanical mixing at ambient temperature. The IF-MoS_2 stability is another advantage. As known from decades of the hydrotreating catalysis research, the edges of MoS_2 slabs bearing catalytic sites are fragile and prone to oxidation. As with IF-MoS_2 systems, they are much more stable and not subjected to rapid oxidation due to their closed-shell structure. Finally, PHER catalysts using mechanical mixtures of commercial titania with small amounts of MoS_2 should be easily scalable to consider their practical use. Extreme simplicity of preparation, sulfur tolerance of MoS_2 and low cost of such catalysts would open ways to investigation of their real-life applications, such as biomass valorization.

References

[1] C. G. Silva, R. Juarez, T. Marino, R. Molinari, H. Garcia, Influence of excitation wavelength (UV or visible light) on the photocatalytic activity of titania containing gold nanoparticles for the generation of hydrogen or oxygen from water, J. Am. Chem. Soc. 133 (2011) 595-602.

[2] J. Liu, Y. Liu, N.Y. Liu, Y. Z. Han, X. Zhang, H. Huang, Y. Lifshitz, S. T. Lee, J. Zhong, Z. H. Kang, Metal-free efficient photocatalyst for stable visible water splitting via a two-electron pathway, Science 347 (2015) 970–974.

[3] M. Ni, M. K. H. Leung, D. Y. C. Leung, K. Sumathy, A review and recent developments in photocatalytic water-splitting using TiO_2 for hydrogen production Renew. Sust. Energy Rev. 11 (2007) 401–425.

[4] M. D. Hernandez-Alonso, F. Fresno, S. Suarez, J. M. Coronado Development of alternative photocatalysts to TiO_2: Challenges and opportunities, Energy Environ. Sci. 2 (2009) 1231-1257.

[5] W. Jones, D. J. Martin, A. Caravaca, A. M. Beale, M. Bowker, T. Maschmeyer, G. Hartley, A. Masters, A comparison of photocatalytic reforming reactions of methanol and triethanolamine with Pd supported on titania and graphitic carbon nitride, App. Catal. B: Environ. 240 (2019) 373-379.

[6] H. Bahruji, M. Bowker, P. R. Davies, J. Kennedy, D.J. Morgan, The importance of metal reducibility for the photoreforming of methanol on transition metal-TiO_2 photocatalysts and the use of non-precious metals, Int. J. Hydr. Energy 40 (2015) 1465-1471.

[7] D. W. Jing, L.J. Guo, WS_2 sensitized mesoporous TiO_2 for efficient photocatalytic hydrogen production from water under visible light irradiation, Catal. Commun. 8 (2007) 795–799.

[8] Y. Zhu, Q. Ling, Y. Liu, H. Wang and Y. Zhu, Photocatalytic H_2 evolution on MoS_2–TiO_2 catalysts synthesized via mechanochemistry, Phys. Chem. Chem. Phys., 2015, 17, 933-940.

[9] W. Gao, M. Wang, C. Ran, L. Li, Facile one-pot synthesis of MoS_2 quantum dots–graphene–TiO_2 composites for highly enhanced photocatalytic properties, Chem. Commun. 51 (2015) 1709 -1712.

[10] B. Chen, Y. Meng, J. Sha, C. Zhong, W. Hu, N. Zhao, Preparation of MoS_2/TiO_2 based nanocomposites for photocatalysis and rechargeable batteries: progress, challenges, and perspective, Nanoscale. 10 (2018) 34–68.

[11] B. Chen, N. Zhao, L. Guo, F. He, C. Shi, C. He, J. Li, E. Liu, Facile synthesis of 3D few-layered MoS_2 coated TiO_2 nanosheet core–shell nanostructures for stable and high-performance lithium-ion batteries, Nanoscale 7 (2015) 12895-12905.

[12] D. Voiry, R. Fullon, J. Yang, C. De Carvalho Castro de Silva, R. Kappera, I. Bozkurt, D. Kaplan, M. J. Lagos, P. E. Batson, G. Gupta, A. D. Mohite, L. Dong, D. Er, V. B. Shenoy, T. Asefa, M. Chhowalla, The role of electronic coupling between substrate and 2D MoS_2 nanosheets in electrocatalytic production of hydrogen, Nat. Mater. 15 (2016) 1003–1009.

[13] H. Li, Y. Wang, G. Chen, Y. Sang, H. Jiang, J. He, X. Li, H. Liu, Few-layered MoS_2 nanosheets wrapped ultra-fine TiO_2 nanobelts with enhanced photocatalytic property, Nanoscale 8 (2016) 6101-6109.

[14] X. Hu, S. Lu, J. Tian, N. Wei, X. Song, X. Wang, H. Cui, The selective deposition of MoS_2 nanosheets onto (101) facets of TiO_2 nanosheets with exposed (001) facets and their enhanced photocatalytic H_2 production, App. Catal. B: Environ. 241 (2019) 329-337.

[15] D. Benetti, K. T. Dembele, J. Benavides, H. Zhao, S. Cloutier, I. Concina, A. Vomiero, F. Rosei, Functionalized multi-wall carbon nanotubes/TiO_2 composites as efficient photoanodes for dye sensitized solar cells, J. Mater. Chem. C, 4 (2016) 3555-3562.

[16] C. Liu, L. Wang, Y. Tang, S. Luo, Y. Liu, S. Zhang, Y. Zeng, Y. Xu, Vertical single or few-layer MoS_2 nanosheets rooting into TiO_2 nanofibers for highly efficient photocatalytic hydrogen evolution, Appl. Catal. B: Environ. 164 (2015) 1–9.

[17] A. B. Laursen, S. Kegnaes, S. Dahl, I. Chorkendorff, Molybdenum sulfides—efficient and viable materials for electro - and photoelectrocatalytic hydrogen evolution, Energy Environ. Sci. 5 (2012) 5577–5591.

[18] H. He, J. Lin, W. Fu, X. Wang, H. Wang, Q. Zeng, Q. Gu, Y. Li, C. Yan, B. K. Tay, C. Xue, X. Hu, S. T. Pantelides, W. Zhou, Z. Liu, MoS_2/TiO_2 Edge-On Heterostructure for Efficient Photocatalytic Hydrogen Evolution, Adv. Energy Mater. 6 (2016) 1600464.

[19] E. Girel, E. Puzenat, C. Geantet, P. Afanasiev, On the photocatalytic and electrocatalytic hydrogen evolution performance of molybdenum sulfide supported on TiO_2, Catal. Today. 292 (2017) 154–163.

[20] R. Tenne, Inorganic nanoclusters with fullerene-like structure and nanotubes, Prog. Inorg. Chem. 50 (2004) 269-315.

[21] Y. Feldman, E. Wasserman, D.J. Srolovitz, R. Tenne, High-Rate, Gas-Phase Growth of MoS_2 Nested Inorganic Fullerenes and Nanotubes, Science 267 (1995) 222-225.

[22] I. Wiesel, H. Arbel, A. Albu-Yaron, R. Popovitz-Biro, J.M. Gordon, D. Feuermann, R. Tenne Synthesis of WS_2 and MoS_2 fullerene-like nanoparticles from solid precursors, Nano Research, 2 (2009) 416-424.

[23] D. M. D. J. Singh, T. Pradeep, J. Bhattacharjee, U. V. Waghmare, Novel Cage Clusters of MoS_2 in the Gas Phase, J. Phys. Chem. A, 109 (2005) 7339–7342.

[24] J. Etzkorn, H.A. Therese, F. Rocker, N. Zink, U. Kolb, W. Tremel, Metal–Organic Chemical Vapor Depostion Synthesis of hollow inorganic-fullerene-type MoS_2 and $MoSe_2$ nanoparticles, Adv. Mater., 17 (2005) 2372-2375.

[25] P. Afanasiev, Topotactic synthesis of size-tuned MoS_2 inorganic fullerenes that allows revealing particular catalytic properties of curved basal planes. Appl. Catal. B: Environ. 227 (2018) 44-53.

[26] A. Nogueira, R. Znaiguia, D. Uzio, P. Afanasiev, G. Berhault, Curved nanostructures of unsupported and Al_2O_3-supported MoS_2 catalysts: Synthesis and HDS catalytic properties. Appl. Catal. A: Gen. 429 (2012) 92-105.

[27] P. Afanasiev, Non-aqueous metathesis as a general approach to prepare nanodispersed materials: Case study of scheelites, J. Solid State Chem. 229 (2015) 112-123.

[28] C. Liu, L. Wang, Y. Tang, S. Luo, Y. Liu, S. Zhang, Y. Zeng, Y. Xu, Vertical single or few-layer MoS_2 nanosheets rooting into TiO_2 nanofibers for highly efficient photocatalytic hydrogen evolution, Appl. Catal. B: Environ. 164 (2015) 1–9.

[29] A. Kachina, E. Puzenat, S. Ould-Chikh, C. Geantet, P. Delichere, P. Afanasiev, A new approach to the preparation of nitrogen doped titania visible light photocatalyst, Chem. Mater. 24 (2012) 636–642.

[30] I. P. Shapiro, Determination of the forbidden zone width from diffuse reflection spectra, Opt. Spektrosk. 4 (1958) 256-260.

[31] J. Tauc, Absorption edge and internal electric fields in amorphous semiconductors, Mater. Res. Bull. 5 (1970) 721-730.

[32] C. Maheu, L. Cardenas, E. Puzenat, P. Afanasiev, C. Geantet, UPS and UV spectroscopies combined to position the energy levels of TiO_2 anatase and rutile nanopowders, Phys. Chem. Chem. Phys. 20 (2018) 25629-25637.

[33] T. A. Kandiel, R. Dillert, L. Robben, D. W. Bahnemann, Photonic efficiency and mechanism of photocatalytic molecular hydrogen production over platinized titanium dioxide from aqueous methanol solutions, Catal.Today 161(2011) 196-201.

[34] G. L. Chiarello, D. Ferri, E. Selli, Effect of the CH_3OH/H_2O ratio on the mechanism of the gas-phase photocatalytic reforming of methanol on noble metal-modified TiO_2, J. Catal. 280 (2011) 168-177.

[35] S. E. Braslavsky, A. M. Braun, A. E. Cassano, A.V. Emeline, M. I. Litter, L. Palmisano, V. N. Parmon, N. Serpone, Glossary of terms used in photocatalysis and radiation catalysis (IUPAC Recommendations 2011), Pure Appl. Chem. 83 (2011) 931–1014.

[36] P. Afanasiev, New approach to the preparation of highly dispersed transition metals sulfides and nitrides, Catal. Today 250 (2015) 134–144.

[37] P. Afanasiev, The influence of reducing and sulfiding conditions on the properties of unsupported MoS_2 -based catalysts, J. Catal. 269 (2010) 269-280.

[38] K. Suttiponparnit, J. Jiang, M. Sahu, S. Suvachittanont, T. Charinpanitkul, P. Biswas, P. Biswas, Role of Surface Area, Primary Particle Size, and Crystal Phase on Titanium Dioxide Nanoparticle Dispersion Properties, Nanoscale Res. Lett. 6 (2011) 6:27

[39] J. Wang, L. Chen,W. Lu, M. Zeng, L. Tan, F. Ren, C. Jiang, L Fu, Direct growth of molybdenum disulfide on arbitrary insulating surfaces by chemical vapor deposition, RSC Adv. 5 (2015) 4364-4367.

[40] A. K. Mishra , K. V. Lakshmi, L. Huang Eco-friendly synthesis of metal dichalcogenides nanosheets and their environmental remediation potential driven by visible light Sci. Rep. 5 (2015) : 15718.

[41] F. Ye, H. Li, H. Yu, S. Chen, X. Quan, Hydrothermal fabrication of few-layer MoS_2 nanosheets within nanopores on TiO_2 derived from MIL-125(Ti) for efficient photocatalytic H_2 evolution, Appl. Surf. Sci. 426 (2017) 177-184.

[42] P. Afanasiev, C. Lorentz, Oxidation of Nanodispersed MoS_2 in Ambient Air: The Products and the Mechanistic Steps, J. Phys. Chem. C 123 (2019) 7486-7494.

[43] M. Fujitsuka, T. Majima, Efficient charge separation on 3D architectures of TiO_2 mesocrystals packed with a chemically exfoliated MoS_2 shell in synergetic hydrogen evolution. P. Zhang, T. Tachikawa, Chem. Commun. 51 (2015) 7187-7190.

[44] X. Zeng, X. Xiao, W. Zhang, C. Wan, H. Wang, Interfacial charge transfer and mechanisms of enhanced photocatalysis of an anatase TiO_2 (0 0 1) -MoS_2 -graphene nanocomposite: A first-principles investigation. Comp. Mater. Sci. 126 (2017) 43-51.

[45] S. Bai, L. Wang, X. Chen, J. Du, Y. Xiong, Chemically exfoliated metallic MoS_2 nanosheets: A promising supporting co-catalyst for enhancing the photocatalytic performance of TiO_2 nanocrystals, Nano Res. 8 (2015) : 175.

[46] M. M. Ali, K. Sandhya, Y. Nair, One-step solvothermal synthesis of carbon doped TiO2-MoS2 heterostructure composites with improved visible light catalytic activity, New. J. Chem. 40 (2016) 8123-8130.

[47] D. B. Nimbalkar, H. Lo, P. V. R. K. Ramacharyulu, S. Ke, Improved photocatalytic activity of RGO/MoS_2 nanosheets decorated on TiO_2 nanoparticles, RSC Adv., 2016, 6, 31661-31667.

[48] M. Shen, Z. Yan, L. Yang, P. Du, J. Zhang, B. Xiang, MoS_2 nanosheet/TiO_2 nanowire hybrid nanostructures for enhanced visible-light photocatalytic activities, Chem. Commun. 50 (2014) 15447–15449 .

[49] Y. J. Yuan, Z. J. Ye, H. W. Lu, B. Hu, Y. H. Li, D. Q. Chen, J. S. Zhong, Z. T. Yu, Z. G. Zou, Constructing Anatase TiO_2 Nanosheets with Exposed (001) Facets/Layered MoS_2 Two-Dimensional Nanojunctions for Enhanced Solar Hydrogen Generation. ACS Catal. 6 (2016) 532-541.

[50] Q. J. Xiang, J. G. Yu, M. Jaroniec, Synergetic effect of MoS_2 and graphene as cocatalysts for enhanced photocatalytic H_2 production activity of TiO_2 nanoparticles, J. Am. Chem. Soc. 134 (2012) 6575–6578.

[51] Y.G. Li, H. L. Wang, L. M. Xie, Y. Y. Liang, G. S. Hong, H. J. Dai, MoS_2 nanoparticles grown on graphene: An advanced catalyst for the hydrogen evolution reaction, J. Am. Chem. Soc. 133 (2011) 7296–7299.

[52] A. Tahira, Z. H. Ibupoto, R. Mazzaro, S. You, V. Morandi, M. M. Natile, M. Vagin, A. Vomiero, Advanced Electrocatalysts for Hydrogen Evolution Reaction Based on Core–Shell MoS_2/TiO_2 Nanostructures in Acidic and Alkaline Media, ACS Appl. Energy Mater. 2 **(**2019) 2053-2062.

[53] J. Nowotny, T. Bak, T. Burg, M. K. Nowotny, L. R. Sheppard, Effect of Grain Boundaries on Semiconducting Properties of TiO_2 at Elevated Temperatures, J. Phys. Chem. C 111 (2007) 9769–9778.

[54] T. Bak, M. K. Nowotny, L. R. Sheppard, J. Nowotny, Mobility of Electronic Charge Carriers in Titanium Dioxide, J. Phys. Chem. C 112 (2008) 12981–12987.

[55] S. Ikeda, N. Sugiyam, S. Murakami, H. Kominami, Y. Kera, H. Noguchi, K. Uosaki, T. Torimoto, B. Ohtani, Quantitative Analysis of Defective Sites in Titanium(IV) Oxide Photocatalyst Powders, Phys. Chem. Chem. Phys. 5 (2003) 778–783.

[56] Kohtani, S.; Kawashima, A.; Miyabe, H. Reactivity of Trapped and Accumulated Electrons in Titanium Dioxide Photocatalysis. Catalysts 7 (2017) 303.

[57] Y. Shiraishi, Y. Togawa, D. Tsukamoto, S. Tanaka, T. Hirai, Highly Efficient and Selective Hydrogenation of Nitroaromatics on Photoactivated Rutile Titanium Dioxide, ACS Catal. 2 (2012) 2475−2481.

[58] F. Amano, M. Nakata, A. Yamamoto, T. Tanaka, Effect of Ti^{3+} Ions and Conduction Band Electrons on Photocatalytic and Photoelectrochemical Activity of Rutile Titania for Water Oxidation, J. Phys. Chem. C 120 (2016) 6467– 6474.

[59] Y. Shiraishi, H. Hirakawa, Y. Togawa, T. Hirai, Noble-Metal-Free Deoxygenation of Epoxides: Titanium Dioxide as a Photocatalytically Regenerable Electron-Transfer Catalyst, ACS Catal. 4 (2014) 1642−1649.

[60] H. Hirakawa, M. Hashimoto, Y. Shiraishi, T. Hirai, Photocatalytic Conversion of Nitrogen to Ammonia with Water on Surface Oxygen Vacancies of Titanium Dioxide. J. Am. Chem. Soc. 139 (2017) 10929−10936.

[61] K. Wang, Z. Wei, B. Ohtani, E. Kowalska, Interparticle electron transfer in methanol dehydrogenation on platinum-loaded titania particles prepared from P25, Catal. Today 303 (2018) 327–333.

[62] G. R. Bamwenda, S. Tsubota, T. Nakamura and M. Haruta, Photoassisted hydrogen production from a water-ethanol solution: a comparison of activities of Au/TiO_2 and Pt/TiO_2, J. Photochem. Photobiol. A 89 (1995) 177–189.

[63] Y. Xu, M.A.A. Schoonen, The absolute energy positions of conduction and valence bands of selected semiconducting minerals, Amer. Mineral. 85 (2000) 543-556.

[64] D. Robert, Photosensitization of TiO_2 by M_xO_y and M_xS_y nanoparticles for heterogeneous photocatalysis applications, Catal Today, 122 (2007) 20-26.

[65] A. Trenczek-Zajac, J. Banas, M. Radecka, Photoactive TiO_2/MoS_2 electrode with prolonged stability, Int. J. Hydr. Energy 43 (2018) 6824-6837.

[66] N. Kaushik, D. Karmakar, A. Nipane, S. Karande, S. Lodha, Interfacial n-Doping Using an Ultrathin TiO_2 Layer for Contact Resistance Reduction in MoS_2, ACS Appl. Mater. Interf. 8 (2016) 256-263

[67] T. Lana-Villarreal, R. Gomez, M. Gonzalez, P. Salvador, Semiconductor Photooxidation of Pollutants Dissolved in Water: A Kinetic Model for Distinguishing between Direct and Indirect Interfacial Hole Transfer. I. Photoelectrochemical Experiments with Polycrystalline Anatase Electrodes under Current Doubling and Absence of Recombination J. Phys. Chem. B 108 (2004) 20278-20290.

[68] Hybrid catalysts for photoelectrochemical reduction of carbon dioxide: a prospective review on semiconductor/metal complex co-catalyst systems J. Zhao, X. Wang, Z. Xu, J. S. C. Loo J. Mater. Chem. A, 2 (2014) 15228-15233.

[69] C. Gambarotti, L. Melone, C. Punta, Carlo. Semiconductors in Organic Photosynthesis, Artificial Photosynthesis, Mohammad Mahdi Najafpour, IntechOpen, DOI: 10.5772/28076.

[70] X. Liu, L. Chen, Q. Liu, J. He, K. Li, W. Yu, J. P. Ao, K. W. Ang, Band alignment of atomic layer deposited TiO_2/multilayer MoS_2 interface determined by x-ray photoelectron spectroscopy, J. Alloys Compd. 698 (2017) 141-146.

[71] P. Jia, R. Guo, W. Pan, C. Huang, J. Tang, X. Liu, H. Qin, Q. Xu, The MoS_2/TiO_2 heterojunction composites with enhanced activity for CO_2 photocatalytic reduction under visible light irradiation, Colloids Surf. A 570 (2019) 306-316.

[72] R. Tang, S. Zhou, T. Ge, Z. Yuan, L. Yin, Layered MoS_2 Coupled MOFs-Derived Dual-Phase TiO_2 for Enhanced Photoelectrochemical Performance J. Mater. Chem. A 5 (2017) 4962-4971.

[73] H. Li, W. Dong, J. Xi, G. Du, Z. Ji, 3D flowerlike TiO_2/GO and TiO_2/MoS_2 heterostructures with enhanced photoelectrochemical water splitting. J. Mater. Sci. 53 (2018) 7609–7620.

[74] K. Gelderman, L. Lee, S. W. Donne, Flat-Band Potential of a Semiconductor: Using the Mott–Schottky Equation, J. Chem. Educ. 84 (2007) 685– 688.

[75] F. Fabregat-Santiago, G. Garcia-Belmonte, J. Bisquert, P. Bogdanoff, A. Zaban, Mott-Schottky Analysis of Nanoporous Semiconductor Electrodes in Dielectric State Deposited on SnO_2(F) Conducting Substrates J. Electrochem. Soc. 150 (2003) E293– E298.

[76] H. Naatz, R. Hoffmann, A. Hartwig, F. La Mantia, S. Pokhrel, L. Mädler, Determination of the Flat Band Potential of Nanoparticles in Porous Electrodes by Blocking the Substrate–Electrolyte Contact, J. Phys. Chem. C 122 (2018) 2796-2805.

[77] M. A. Butler, D. S. Ginley, Prediction of Flatband Potentials at Semiconductor-Electrolyte Interfaces from Atomic Electronegativities, J. Electrochem. Soc. 125 (1978) 228-232.

[78] S. M. Ahmed, Surface and photoelectrochemical studies of semiconducting MoS_2, Electrochim. Acta, 27 (1982) 707-712.

[79] B. Ohtani, Titania Photocatalysis beyond Recombination: A Critical Review, Catalysts 3 (2013) 942-953.

[80] A. Nitta, M. Takashima, M. Takase, B. Ohtani, Identification and characterization of titania photocatalyst powders using their energy-resolved distribution of electron traps as a fingerprint, Catal. Today 321–322 (2019) 2-8.

[81] C. R. López, E. P. Melián, J.A. Ortega Méndez, D. E. Santiago, J.M. Doña Rodríguez, O. González Díaz, Comparative study of alcohols as sacrificial agents in H_2 production by heterogeneous photocatalysis using Pt/TiO_2 catalysts, J. Photochem. Photobiol. A: Chem. 312 (2015) 45-54.

[82] A. A. Ismail, D. W. Bahnemann, I. Bannat, M. Wark, Gold Nanoparticles on Mesoporous Interparticle Networks of Titanium Dioxide Nanocrystals for Enhanced Photonic Efficiencies J. Phys. Chem C 113 (2009) 7429-7435.

[83] C. Y. Wang, R. Pagel, J. K. Dohrmann, D. W. Bahnemann, Antenna mechanism and deaggregation concept: novel mechanistic principles for photocatalysis, C. R. Chimie 9 (2006) 761-773.

[84] O. A. Semenikhin, V. E. Kazarinov, L. Jiang, K. Hashimoto, A. Fujishima, Suppression of Surface Recombination on TiO_2 Anatase Photocatalysts in Aqueous Solutions Containing Alcohol, Langmuir 15 (1999) 3731-3737.

[85] T. A. Kandiel, R. Dillert, L. Robben, D. W. Bahnemann, Photonic efficiency and mechanism of photocatalytic molecular hydrogen production over platinized titanium dioxide from aqueous methanol solutions, Catal. Today 161 (2011) 196–201.

[86] A. A. Ismail, D. W. Bahnemann, L. Robben, V. Yarovyi, M. Wark, Palladium Doped Porous Titania Photocatalysts: Impact of Mesoporous Order and Crystallinity, Chem. Mater. 22 (2010) 108-116.

[87] A. Mills, M. Bingham, C. O'Rourke, M. Bowker, Modelled kinetics of the rate of hydrogen evolution as a function of metal catalyst loading in the photocatalysed reforming of methanol by Pt (or Pd)/TiO2, J. Photochem. Photobiol. A: Chem. 373 (2019) 122-130.

[88] J. Tang, J. R. Durrant, D. R. Klug, Mechanism of Photocatalytic Water Splitting in TiO_2. Reaction of Water with Photoholes, Importance of Charge Carrier Dynamics, and Evidence for Four-Hole Chemistry, J. Am. Chem. Soc. 130 (2008) 13885–13891.

[89] K. T. Dembele, G. S. Selopal, R. Milan, C. Trudeau, D. Benetti, A. Soudi, M. M. Natile, G. Sberveglieri, S. Cloutier, I. Concina, F. Rosei, A. Vomiero, Graphene below the percolation threshold in TiO_2 for dye-sensitized solar cells, J. Mater. Chem. A 3 (2015) 2580-2588.

[90] G. Wang, H. Wang, Y. Ling, Y. Tang, X. Yang, R. C. Fitzmorris, C. Wang, J. Z. Zhang, Y. Li, Hydrogen-treated TiO_2 nanowire arrays for photoelectrochemical water splitting, Nano Lett. 11 (2011), 3026-3033.

[91] F. M. Pesci, G. Wang D. R. Klug, Y. Li, A. J. Cowan, Efficient suppression of electron–hole recombination in oxygen-deficient hydrogen-treated TiO_2 nanowires for photoelectrochemical water splitting, J. Phys. Chem. C 117 (2013) 25837-25844.

[92] C. Dessal, L. Martínez, C. Maheu, T. Len, F. Morfin, J.L. Rousset, E. Puzenat, P. Afanasiev, M. Aouine, L. Soler, J. Llorca, L. Piccolo, Influence of Pt particle size and reaction phase on the photocatalytic performances of ultradispersed Pt/TiO_2 catalysts for hydrogen evolution, J Catal. 375 (2019) 155-163.

Graphical abstract